Dark excitons due to direct Coulomb interactions in silicon quantum dots

F. A. Reboredo, A. Franceschetti, and A. Zunger
National Renewable Energy Laboratory, Golden, Colorado 80401
(Received 4 May 1999)

Electron-hole exchange interactions can lead to spin-forbidden ''dark'' excitons in direct-gap quantum dots. Here, we explore an alternative mechanism for creating optically forbidden excitons. In a large spherical quantum dot made of a diamond-structure semiconductor, the symmetry of the valence band maximum (VBM) is t_2. The symmetry of the conduction band minimum (CBM) in direct-gap material is a_1, but for indirect-gap systems the symmetry could be (depending on size) a_1, e, or t_2. In the latter cases, the resulting manifold of excitonic states contains several symmetries derived from the symmetries of the VBM and CBM (e.g., $t_2 \times t_2 = A_1 + E + T_1 + T_2$ or $t_2 \times e = T_1 + T_2$). Only the T_2 exciton is optically active or ''bright,'' while the others A_1, E, and T_1 are ''dark.'' The question is which is lower in energy, the *dark* or *bright*. Using pseudopotential calculations of the single-particle states of Si quantum dots and a direct evaluation of the screened electron-hole Coulomb interaction, we find that, when the CBM symmetry is t_2, the direct electron-hole Coulomb interaction lowers the energy of the *dark* excitons relative to the *bright* T_2 exciton. Thus, the lowest energy exciton is forbidden, even without an electron-hole exchange interaction. We find that our *dark-bright* excitonic splitting agrees well with experimental data of Calcott *et al.*, Kovalev *et al.*, and Brongersma *et al.* Our excitonic transition energies agree well with the recent experiment of Wolkin *et al.* In addition, and contradicting simplified models, we find that Coulomb correlations are more important for small dots than for intermediate sized ones. We describe the full excitonic spectrum of Si quantum dots by using a many-body expansion that includes both Coulomb and exchange electron hole terms. We present the predicted excitonic spectra.

I. INTRODUCTION

Much of the interest in semiconductor quantum dots (QD's) centers around the ability to tune their emission energy and intensity via their quantum size. For that purpose, it is desirable to have *allowed* excitonic transitions at threshold. However, it is possible that quantum size effects will make the lowest excitonic transitions *forbidden* (''dark''). The first such case is due to electron-hole exchange effects in dots made of a direct-gap zinc-blende material.[1–5] In this case, the valence band maximum (VBM) has t_2 symmetry (derived from the bulk Γ_{15} state), whereas the conduction band minimum (CBM) is a_1 (derived from the bulk Γ_1 state). Consequently, in the absence of the electron-hole interaction, the exciton has the symmetry $t_2 \times a_1 = T_2$, and the corresponding transition is optically allowed. The electron-hole exchange interaction can split T_2 into a *lower-energy* triplet and a higher-energy singlet. Whereas the spin-orbit interaction can mix singlets and triplets, the lowest state is still forbidden. Indeed, for direct-gap QD's, the only mechanism to have a forbidden, ''dark exciton'' is through such exchange interaction. The second case explored here is when the bulk material from which the QD is made is a multivalley semiconductor (Si, Ge, AlAs, GaP), or when the QD becomes indirect because of quantum confinement (e.g., small GaAs dots are predicted to have an indirect gap[6]). Then, the CBM electron state need not have a_1 symmetry, but can also be t_2 or e.[7–9] In Table I, we give the symmetries of the possible excitons (capital letters) based on the symmetries of the single-particle hole and electron wave functions (lowercase letters). For example, if both the hole and the electron have t_2 symmetry, one can get $t_2 \times t_2 = T_1 + T_2 + E + A_1$ excitons. In the absence of electron-hole Coulomb attraction, all four states are degenerate. However, only T_2 is allowed while the T_1, E, and A are dark. In direct-gap materials, Coulomb interactions tend to shift states, but not to split them. Here we ask whether in indirect-gap dots the electron-hole Coulomb interaction (not the exchange) can split the energy of a dark exciton (T_1, E, or A_1) below the energy of the ''bright'' T_2 exciton. We address this question for Si quantum dots. To answer this question we must know (1) the symmetries and energies of the near-edge single-particle electron and hole states, (2) the matrix elements of the electron-hole direct Coulomb and exchange interactions between them, and (3) the screening function. All of these quantities can depend on the size and shape of the dot.

Silicon dots can be prepared via electrochemical etching,[10] reactive sputtering,[11] embedding in sol-gel matrices,[12] implantation in a SiO_2 layer,[13] self-assembly,[14,15]

TABLE I. Possible symmetries of the excitons as a result of the symmetry of the electron and hole wave functions. An asterisk denotes allowed (bright) excitons.

Case		Hole	Electron	Possible excitons
I	*a*	t_2	t_2	$T_1 + T_2^* + E + A_1$
I	*b*	t_2	a_1	T_2^*
I	*c*	t_2	e	$T_1 + T_2^*$
II	*d*	t_1	t_2	$T_1 + T_2^* + E + A_2$
II	*e*	t_1	a_1	T_1^*
II	*f*	t_1	e	$T_1 + T_2^*$

inverse micelles synthesis,[16] and thermal vaporization.[17] The most popular experiments that probe QD's are optical measurements,[10,11,17] in which an electron-hole pair (an exciton) is generated in the QD by the incoming photons. The physics of the experiment is dominated by the electron and hole energy levels, the electron-hole Coulomb interaction, and the response or screening of the rest of the electrons in the valence band.

The classical theoretical approach to the problem is the effective mass approximation (EMA), which predicts that the shift in the single-particle energy gap scales as $1/R^2$ with the radius R of a quantum dot. The EMA and a size-independent screening assumption predict that the Coulomb energy scales as $1/R$ in the limit $R\rightarrow 0$. However, recent microscopic calculations,[7,8,18–22] show that the single-particle energy gap dependence on R is less strong. This is due mainly to band mixing and nonparabolicity effects. In addition, the Coulomb binding energies are expected to increase faster than $1/R$ because the dielectric screening becomes less efficient than in the bulk.[23–25]

In the past, the calculation of energy levels of QD's was also performed using EMA,[26] empirical tight binding,[7,18–20] empirical pseudopotential methods,[1,3,22] and local density approximation.[8,24] The symmetry of the band-edge wave functions has been discussed in detail by Ren[7,9] and Delley *et al.*[8] However, the symmetry of the exciton was not discussed. The excitonic spectra of spherical Si QD have been studied in the frame of the EMA (Ref. 26) and empirical tight binding.[18,19] But, the exciton in Si has not been calculated in a configuration interaction pseudopotential frame.

In this paper, we first calculate the single-particle states using a pseudopotential approach. In agreement with previous calculations,[7,8] we find that the symmetry of the CBM can be a_1, e, or t_2, depending on the QD radius, whereas the symmetry of the VBM is in general t_2 (but could be t_1 for a sufficiently small QD). We next calculate the electron-hole interaction matrix elements using microscopic pseudopotential wave functions and find that the excitonic gap is in excellent agreement with recent experimental results.[10] We also find that (1) the symmetry of the lowest excitonic transition is determined by the symmetry of the single-particle states and not by the size of the dot. (2) If the CBM is t_2, the direct Coulomb interaction alone can split the exciton manifold $T_1+T_2+E+A_1$ into lower-energy dark states and higher-energy bright states. At low temperatures, only the lowest-energy (dark) excitons are populated, so emission is weak and long-lived. At higher temperatures, all excitons are populated but only the T_2 emit. (3) On the other hand, if the CBM is a_1 or e symmetric, then the lower-energy exciton has T_2 symmetry, which is optically allowed. (4) Even if the VBM is t_1 and the CBM is t_2, the lowest exciton can still be dark because the Coulomb interaction lowers a non-T_2 state below T_2. (5) Simple EMA models suggest that the single-particle gap scales with size as $\varepsilon_g \sim R^{-2}$, whereas for a size-independent screening, the electron-hole Coulomb interaction is expected to scale as $J_{eh}\sim R^{-1}$. We find, in contrast with this simple expectation, $\varepsilon_g \sim R^{-1.2}$ and $J_{eh}\sim R^{-1.5}$. Thus, in contradiction to simple theories, we find that when the dot size is much smaller than the bulk-exciton Bohr radius, the Coulomb interactions are more important than the single-particle splittings. Therefore, configuration-interactions can produce reorderings in the symmetries of the excitonic states in smaller dots with respect to the uncorrelated states. (6) Our configuration-interaction calculations including both Coulomb and exchange interactions provides a prediction for the excitonic manifold in spherical Si dots.

II. METHOD OF CALCULATION

A. Calculation and classification of single-particle energies and wave functions

We consider approximately spherical silicon crystallites centered around a Si atom. All Si atoms are assumed to be located at their ideal bulk positions. The dots are generated by discarding all the Si atoms that are outside a sphere of a given radius. We eliminate surface atoms that have more than two dangling bonds, while the remaining dangling bonds are passivated with hydrogen atoms, as described in Ref. 27. All the dots generated by this procedure have T_d symmetry. The passivated dots are then surrounded by vacuum and placed in a large supercell, which is repeated periodically. The closest distance between two neighboring dots is always larger than 10 Å. Having created an (artificial) periodic structure, we can calculate its electronic structure via ordinary ''band structure'' methods applied to the supercell. We consider dots with radii ranging from 7.5 to 27.25 Å and containing 87 to 4235 Si atoms (shown in the first two columns of Table II).

The single-particle energy levels and wave functions are obtained by solving the Schrödinger equation

$$H\,\psi_i=\varepsilon_i\,\psi_i, \tag{1}$$

where the Hamiltonian is given by[22]

$$H=-\frac{\hbar^2}{2m}\nabla^2+\sum_{\mathbf{R}_{Si}} v_{Si}(\mathbf{r}-\mathbf{R}_{Si})+\sum_{\mathbf{R}_H} v_H(\mathbf{r}-\mathbf{R}_H). \tag{2}$$

Here m is the bare electron mass, and v_{Si} and v_H are the atomic local empirical pseudopotentials[22] of Si and H, which are taken from Refs. 22 and 27.

We expand the wave functions $\psi(\mathbf{r})$ in a plane wave basis set. The energy cutoff must be compatible with the cutoff used in generating the pseudopotentials[22,27] v_{Si} and v_H, which were designed for 4.5 Ry cutoff. We solve Eq. (1) using the folded-spectrum method[22] to obtain the states near the band edges. Thus, our method is not self-consistent. However, the use of screened pseudopotentials makes it appropriate for large dots.

Because the dot has T_d symmetry, its single-particle states must belong to the irreducible representations a_1, a_2, e, t_1, or t_2. The single-particle states that belong to the representations a_1 or a_2 of the T_d group are in general nondegenerate, whereas those that belong to e, t_1, and t_2 are degenerate. The symmetry of any solution $\psi(\mathbf{r})$ of Eq. (1) can be found by using an operator $P^{(\mu)}$ that projects any function into the subspace of the representation μ:[28]

$$P^{(\mu)}=\frac{n_\mu}{g}\sum_Q \chi_Q^{(\mu)*}\hat{O}_Q, \tag{3}$$

TABLE II. CBM and VBM energies and symmetries for different Si QD radius.

Radius (Å)	Si atoms	CBM		VBM		Band gap (eV)
		Energy (eV)	Symmetry	Energy (eV)	Symmetry	
7.46	87	−2.65	$a1$	−5.97	$t2$	3.32
8.37	123	−2.91	e	−5.92	$t1$	3.00
8.89	147	−2.87	$t2$	−5.80	$t1$	2.93
10.03	211	−3.06	$t2$	−5.75	$t1$	2.69
12.70	429	−3.28	$t2$	−5.51	$t2$	2.22
13.48	513	−3.32	e	−5.44	$t2$	2.12
15.07	717	−3.41	$a1$	−5.40	$t2$	1.99
16.21	891	−3.46	$a1$	−5.35	$t2$	1.89
16.72	979	−3.46	$t2$	−5.33	$t2$	1.87
17.32	1087	−3.49	$t2$	−5.30	$t2$	1.81
17.51	1123	−3.49	$t2$	−5.30	$t2$	1.81
17.93	1207	−3.50	$a1$	−5.30	$t2$	1.79
18.75	1379	−3.53	e	−5.27	$t2$	1.74
19.38	1551	−3.54	e	−5.25	$t2$	1.71
20.27	1743	−3.56	$a1$	−5.22	$t2$	1.66
20.72	1863	−3.57	$t2$	−5.21	$t2$	1.64
21.64	2121	−3.59	$a1$	−5.20	$t2$	1.61
23.14	2593	−3.61	$t2$	−5.17	$t2$	1.56
24.42	3049	−3.63	e	−5.16	$t2$	1.52
27.25	4235	−3.66	$a1$	−5.12	$t2$	1.46

where n_μ is the dimension of the subspace of the representation μ, g is the total number of operations Q in the symmetry group, $\chi_Q^{(\mu)}$ is the character corresponding to the operation Q in the representation μ, and $\hat{O}_Q$ is an operator that applies the transformation Q of the group to the wave function $\psi(\mathbf{r})$. Then we calculate the matrix element

$$p(\psi,\mu)=\frac{\langle\psi|P^{(\mu)}|\psi\rangle}{\langle\psi|\psi\rangle}. \tag{4}$$

Because $P^{(\mu)}$ is a projector,[28] $p(\psi,\mu)$ is only going to be equal to 1 if ψ belongs to the representation μ of the group.

B. The many-body expansion

From the solutions of Eq. (1) we construct a set of single-substitution Slater determinants $\{\Phi_{e,h}\}$, obtained from the ground-state Slater determinant Φ_0 by promoting an electron from the (occupied) valence state ψ_h of energy ε_h to the (unoccupied) conduction state ψ_e of energy ε_e:

$$\Phi_0(\mathbf{r}_1,\sigma_1,\ldots,\mathbf{r}_N,\sigma_N) = \mathcal{A}[\psi_1(\mathbf{r}_1,\sigma_1)\cdots\psi_h(\mathbf{r}_i,\sigma_i)\cdots\psi_N(\mathbf{r}_N,\sigma_N)] \tag{5}$$

$$\Phi_{h,e}(\mathbf{r}_1,\sigma_1,\ldots,\mathbf{r}_N,\sigma_N) = \mathcal{A}[\psi_1(\mathbf{r}_1,\sigma_1)\cdots\psi_e(\mathbf{r}_i,\sigma_i)\cdots\psi_N(\mathbf{r}_N,\sigma_N)]. \tag{6}$$

Here, N is the total number of electrons in the system, $\sigma=\uparrow,\downarrow$ is the spin variable, and $\mathcal{A}$ is the antisymmetrizing operator. The Slater determinant $\Phi_{h,e}$ represents an electron-hole pair. Two Slater determinants Φ_{h_1,e_1} and Φ_{h_2,e_2} belong to the same ''configuration'' if the single-particle hole states ψ_{h_1} and ψ_{h_2} are degenerate ($\varepsilon_{h_1}=\varepsilon_{h_2}$), and the single-particle electron states ψ_{e_1} and ψ_{e_2} are degenerate ($\varepsilon_{e_1}=\varepsilon_{e_2}$).

The exciton wave functions $\Psi^{(\alpha)}$ are expanded in terms of this determinantal basis set[1,29]

$$\Psi^{(\alpha)}=\sum_{e=1}^{Ne}\sum_{h=1}^{N_h} C_{h,e}^{(\alpha)}\Phi_{h,e}, \tag{7}$$

where N_h and N_e denote the number of hole and electron states included in the expansion of the exciton wave functions. In this notation, the hole states are numbered from 1 to N_h in order of *decreasing* energy starting from the VBM, whereas the electron states are numbered from 1 to N_e in order of *increasing* energy starting from the CBM.

The matrix elements of the many-particle Hamiltonian $\mathcal{H}$ in the basis set $\{\Phi_{h,e}\}$ are calculated as

$$\mathcal{H}_{he,\,h'e'}\equiv\langle\Phi_{he}|\mathcal{H}|\Phi_{h'e'}\rangle=(\varepsilon_e-\varepsilon_h)\,\delta_{h,h'}\,\delta_{e,e'}-J_{he,\,h'e'} + K_{he,\,h'e'} \tag{8}$$

where J and K are the electron-hole Coulomb and exchange integrals, respectively

$$J_{he,h'e'}=e^2\sum_{\sigma_1,\sigma_2}\int\int\frac{\psi^*_{h'}(\mathbf{r}_1,\sigma_1)\psi^*_e(\mathbf{r}_2,\sigma_2)\psi_h(\mathbf{r}_1,\sigma_1)\psi_{e'}(\mathbf{r}_2,\sigma_2)}{\overline{\epsilon}(|\mathbf{r}_1-\mathbf{r}_2|,R)|\mathbf{r}_1-\mathbf{r}_2|}d\mathbf{r}_1\,d\mathbf{r}_2, \tag{9}$$

$$K_{he,h'e'}=e^2\sum_{\sigma_1,\sigma_2}\int\int\frac{\psi^*_{h'}(\mathbf{r}_1,\sigma_1)\psi^*_e(\mathbf{r}_2,\sigma_2)\psi_{e'}(\mathbf{r}_1,\sigma_1)\psi_h(\mathbf{r}_2,\sigma_2)}{\overline{\epsilon}(|\mathbf{r}_1-\mathbf{r}_2|,R)|\mathbf{r}_1-\mathbf{r}_2|}d\mathbf{r}_1\,d\mathbf{r}_2. \tag{10}$$

The excitonic states of the quantum dot are obtained by solving the secular equation:

$$\sum_{h'=1}^{N_v}\sum_{e'=1}^{N_c}\mathcal{H}_{he,h'e'}\,C^{(\alpha)}_{h',e'}=E^{(\alpha)}\,C^{(\alpha)}_{h,e}. \tag{11}$$

The Hamiltonian matrix of Eq. (11) is shown schematically in Fig. 1. The diagonal blocks (shaded areas) correspond to matrix elements $\mathcal{H}_{he,\,h'e'}$ between Slater determinants belonging to the *same* configuration. Each block corresponds to a row in Table I. For example, if the hole state is t_2 and the electron state is a_1, the $t_2\times a_1$ block is (including spin) 12×12. In a similar way, the $t_2\times t_2$ block is 36×36. The off-diagonal blocks (unshaded areas) describe the coupling between different configurations (i.e., correlation effects).

In order to obtain an insight about the origin of the calculated excitation energies, we will first solve the single configuration problem by including only the diagonal blocks of Fig. 1 in the many-body Hamiltonian [Eq. (11)]. This will be done in two steps: (1) retaining only the direct Coulomb interaction J, and then (2) including both Coulomb J and exchange K interactions. We will then introduce configuration mixing (correlations) by including the off-diagonal blocks in Fig. 1.

C. The model screening dielectric function

In Eqs. (9) and (10) we have screened the electron hole interaction by a dielectric function $\overline{\epsilon}(|\mathbf{r}_1-\mathbf{r}_2|,R)$. The need for this screening can be explained as follows. Imagine that we had solved self-consistently a single-particle Hartree-Fock equation instead of the empirical pseudopotential Hamiltonian in Eq. (1). The solution would depend on the assigned occupation numbers $\{n_h,n_e\}$ for all the hole (h) and electron (e) levels of the dot. In the ground state $\{n^o_h,n^o_e\}$ all the electron and hole levels are empty. We can now create a specific electron-hole pair by removing an electron from a particular level in the valence band and placing it in a particular level in the conduction band. The new occupation numbers are $\{\tilde{n}_h,\tilde{n}_e\}$. If we had self-consistently solved the Hartree-Fock equation for the new occupation numbers we would have obtained new single-particle wave functions $\{\tilde{\psi}\}$, and therefore, new Hartree and exchange potentials. In practice, we do not solve the problem self-consistently. Instead, we think of the new wave functions $\{\tilde{\psi}\}$ as linear combinations of the old wave functions $\{\psi^o\}$. Specifically, every wave function in $\{\tilde{\psi}\}$ now contains a mixture from all states:

$$\tilde{\psi}_h=\psi^o_h+\sum_{h'}a_{h,h'}\psi^o_{h'}+\sum_{e'}a_{h,e'}\psi^o_{e'}$$
$$\tilde{\psi}_e=\psi^o_e+\sum_{h'}a_{e,h'}\psi^o_{h'}+\sum_{e'}a_{e,e'}\psi^o_{e'}. \tag{12}$$

When one constructs the CI expansion of Eq. (8) one should incorporate not only the many-body function Φ due to ψ^o_h and ψ^o_e, but also all the cross terms resulting from the second and third sums in Eq. (12). These cross terms describe double, triple, etc., electron-hole pairs that *screen* or ''dress'' a particular electron-hole excitation. We thus see that the wave-function-mixing affects both electron-hole Hartree and electron-hole exchange interaction. In our CI expansion all these multiple electron-hole pairs are neglected. To correct for this, one introduces the screening $\overline{\epsilon}(|\mathbf{r}_1-\mathbf{r}_2|,R)$ in Eqs. (9) and (10).

To model this screening, we first assume that the effect of excitation-induced wave-function-mixing can be thought of as an effect of some external field, so that the self-consistent field approximation[30] can be applied. Second, we assume linear response. Thus *multiple* electron-hole excitations will

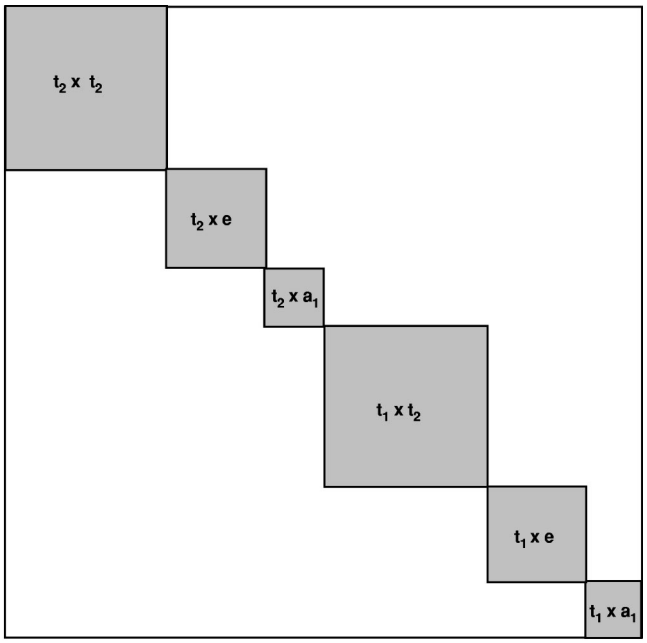

FIG. 1. Schematic description of the configuration interaction matrix of Eq. (11). The shaded areas correspond to matrix elements between Slater determinants belonging to the same configuration, and off-diagonal blocks represent configuration mixing, which produces correlation effects.

be described by a single screening function $\bar{\epsilon}(|\mathbf{r}_1-\mathbf{r}_2|,R)$. Third, we choose an analytical approximation for $\bar{\epsilon}(|\mathbf{r}_1-\mathbf{r}_2|,R)$ which is described in Ref. 31.

Our foregoing argument suggests that the exchange interaction must also be screened. In the past, it was believed that while the Coulomb interaction is long-ranged (LR) and therefore must be screened, the exchange interaction is purely short-ranged and therefore should remain unscreened. We have recently shown[1] that, in quantum dots, there is a significant LR component to the exchange. Since our dielectric function $\bar{\epsilon}(|\mathbf{r}_1-\mathbf{r}_2|,R)$ will approach 1 at small $|\mathbf{r}_1-\mathbf{r}_2|$ it will naturally leave the SR interactions unscreened. However, the LR exchange interactions will be screened. This is further discussed in Ref. 1.

The electron-hole Coulomb and exchange integrals of Eqs. (9) and (10) thus involve a screening function $\bar{\epsilon}(\mathbf{r}_1,\mathbf{r}_2,R)$ that depends on the interparticle distance $|\mathbf{r}_1-\mathbf{r}_2|$ and on the quantum dot radius R.[1] Because there is a discontinuity in the dielectric function at the surface of the dots, surface-polarization energies should be taken into account. However, it has been shown that the electron and hole self-polarization energies and the electron-hole polarization energy cancel each other almost exactly both in spherical[32] and cubic[33] dots. Therefore, polarizations effects will not be considered in the present case.

Approximating $\bar{\epsilon}(\mathbf{r}_1,\mathbf{r}_2,R)\approx\bar{\epsilon}(|\mathbf{r}_1-\mathbf{r}_2|,R)$, the screened Coulomb potential of Eqs. (9) and (10) can be rewritten as

$$g(|\mathbf{r}_1-\mathbf{r}_2|)\equiv\frac{e^2}{\bar{\epsilon}(|\mathbf{r}_1-\mathbf{r}_2|)|\mathbf{r}_1-\mathbf{r}_2|}$$
$$=e^2\int\epsilon^{-1}(|\mathbf{r}_1-\mathbf{r}|)|\mathbf{r}-\mathbf{r}_2|^{-1}\,d\mathbf{r}, \qquad (13)$$

where ϵ^{-1} is the inverse dielectric function. The Fourier transform of the screened Coulomb potential is

$$g(k)=\epsilon^{-1}(k)\frac{4\pi e^2}{k^2}, \qquad (14)$$

where $\epsilon^{-1}(k)$ is the Fourier transform of $\epsilon^{-1}(|\mathbf{r}_1-\mathbf{r}|)$. Because silicon is a covalent semiconductor, there is no ionic contribution to the screening. We construct a model dielectric function as follows: the inverse dielectric constant ϵ^{-1} consists of the electronic (high-frequency) contribution only, which is approximated here by the Thomas-Fermi model proposed by Resta[31]

$$\epsilon^{-1}(k)=\frac{k^2+q^2\sin(k\rho_\infty)/(\epsilon_\infty^{dot}k\rho_\infty)}{k^2+q^2}. \qquad (15)$$

Here $q=2\pi^{-1/2}(3\pi^2n_0)^{1/3}$ is the Thomas-Fermi wave vector (where n_0 is the average valence band electron density), and ρ_∞ is the solution of the equation $\sinh(q\rho_\infty)/(q\rho_\infty)=\epsilon_\infty^{dot}$. The *macroscopic* dielectric constant of the quantum dot ϵ_∞^{dot} is related to the polarizability of the quantum dot as a whole. The dielectric constant ϵ_∞^{dot} is obtained from an interpolation of the results of the screening dielectric constant using a moments method[23] and pseudopotential calculations of the wave functions and energy levels for different dot radii:

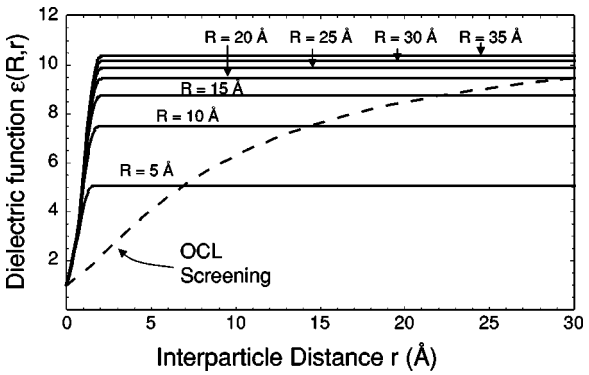

FIG. 2. Dielectric screening for dots. Continuous line: screening function used in this work as a function of the interparticle distance r for different dot radii R. Dashed line: screening function used by Ögüt, Chelikowsky, and Louie (Ref. 24).

$$\epsilon_\infty^{dot}(R)=1+\frac{\varepsilon_0-1}{1+(R_0/R)^\eta}, \qquad (16)$$

where ε_0 is the bulk dielectric constant and R_0 and η are constants. A direct calculation of $\epsilon_\infty^{dot}(R)$ by the pseudopotential method gives for Si $R_0=6.9$ Å and[23] $\eta=1.37$. This expression gives slightly larger values of $\epsilon_\infty^{dot}(R)$ than the one calculated by Lannoo *et al.*[25] (using a self-consistent extended tight binding that incorporates the Coulomb interaction) and also by Ögüt *et al.*[24] (using an LDA calculation and infinitesimal field method in small clusters).

Although the reciprocal space formula for the screening [Eq. (15)] is very useful for our plane wave approach, it is instructive to analyze the real-space screening function $[\bar{\epsilon}(r,R)]$, which is related to $\epsilon^{-1}(k)$ via Eq. (13)

$$\bar{\epsilon}(r,R)=\begin{cases}\epsilon_\infty^{dot}(R)q/[\sinh q(\rho_\infty-r)+q\,r], & r\leqslant\rho_\infty\\ \epsilon_\infty^{dot}(R), & r>\rho_\infty.\end{cases} \qquad (17)$$

Figure 2 shows the dependence of the screening function $\bar{\epsilon}(r,R)$ on the interparticle distance r for different values of the effective radius of the dot R. We have used $\varepsilon_0=11.4$, and a valence electron density $n_0=0.1998$ Å^{-3}. We see that for interparticle distances larger than $\sim$2.5 Å (corresponding to the screening radius ρ_∞) the screening function is identical to its asymptotic value $\epsilon_\infty(R)$. However, for smaller distances it falls quickly to 1. The electron-hole Coulomb interaction is long ranged, so it is essentially screened by the quantum-dot macroscopic dielectric constant ϵ_∞^{dot}. The electron-hole exchange interaction, on the other hand, consists of both a short-range and a long-range component. Because $\bar{\epsilon}(\mathbf{r}_1-\mathbf{r}_2,R)\to1$ when $|\mathbf{r}_1-\mathbf{r}_2|\to0$ (see Fig. 2), the short-range component of the exchange interaction is effectively unscreened, as it is in bulk semiconductors.[34,35] The long-range component, instead, is significantly screened, as discussed in Ref. 1.

The screening function proposed by Resta[31] provides an accurate description of the screening in the bulk.[36] Accord-

ingly, any approximation for the screening function $\epsilon(r,R)$ for a dot should converge to the form given by Resta for all values of r when the dot size R goes to infinity. Figure 2 shows that our screening function has this property. In Fig. 2, we have also plotted the distance dependent screening function used by Ögüt *et al.*[24] In that work, it is assumed that $\bar{\epsilon}(r,R)=\epsilon_{\infty}^{dot}(r)$. This assumption gives a screening function that depends only on the interparticle distance r (independent of the size of the dot). Figure 2 shows that in the approximation used by Ögüt *et al.* $\bar{\epsilon}(r)$ is only equal to the bulk value when the interparticle distance r is infinity. For all other r, the screening function used by Ögüt *et al.* is significantly different. It thus does not describe bulk screening correctly.

D. Comparison of the present method with other approaches

The present method differs form the classical EMA treatment of free-standing QD's (Refs. 2 and 26) in several ways: (1) The present method provides the microscopic structure of the wave functions, not just the envelope structure. (2) It does not require the wave function to vanish at the boundaries of the QD. (3) The numerical solution of Eq. (1) allows us to include unlimited multiband couplings. (4) The method describes the true physical symmetries of the dot (recall that even the most perfect Si QD does not have spherical symmetry, as assumed in the EMA, but rather T_d symmetry).

As to comparison of the present method and tight binding, we note that both methods can give equivalent results if the tight-binding basis is large enough. However (1), the description of the wave function is variationally much more direct and flexible in the plane-wave pseudopotential method; and (2) while the position-dependent wave functions are in general not accessible to a tight-binding model (only the expansion coefficients are), the pseudopotential approach provides the wave functions. Moreover, the method is constrained to give the bulk wave functions that fit local-density approximations (LDA) calculations.

The configuration-interaction formalism used in this work is similar to those followed by Hill *et al.*,[18] Leung *et al.*,[19] and Chamarro *et al.*[5] The main differences appear in the evaluation of the matrix elements in Eqs. (9) and (10): (1) We evaluate the J and K integrals explicitly in terms of the wave functions ψ obtained by solving the quantum dot Hamiltonian [Eq. (1)]. (2) In the works of Chamarro *et al.*,[5] Hill *et al.*,[18] and Leung *et al.*,[19] the exchange integrals are not screened and only interactions up to first neighbors are taken into account while longer-range interactions were neglected. (3) In the work of Leung *et al.*,[19] the Coulomb interaction was screened by a *bulk* distance-dependent dielectric constant that does not depend on the QD radius.

III. RESULTS

A. Single-particle energies and wave functions

Figure 3 shows the cross section of the band-edge wave functions for a few cases. We see that the amplitude of the oscillations in the wave functions is larger around the dot center. The wave-function amplitude on the surface is small, so the wave function and eigenenergies are expected to be rather insensitive to small changes in the surface shape or passivation (see below).

Table II gives the energies and the symmetries obtained by applying Eq. (4) of the band-edge states of dots with different sizes. In agreement with Ren,[7] we found that the VBM symmetry changes from t_2 to t_1 in small dots ($R<12.7$ Å). For even smaller dots ($R<7.5$ Å), the t_2 symmetry of the VBM is restored. However, in our calculations, the t_2 to t_1 crossing occurs at sizes larger than those reported by Ren.[7] The t_2 to t_1 crossing was observed Delley *et al.*[8] only in very small clusters (the cases of 17 and 4 Si atoms). The crossing occurs when the clusters are so small that most of the atoms are in the vicinity of the surface. We cannot be sure about the results obtained for those small clusters.

With respect to the CBM, we confirm the observation made in previous calculations[7,8] that the symmetry changes between the a_1, e, and t_2 representations in an irregular way. The energy-splitting between these three states (ΔE) approaches zero for large R (e.g., $\Delta E=20$ meV for $R=13.48$ Å , $\Delta E=4.1$ meV for $R=27.25$ Å). We also found that the symmetries are not affected by small (5%) changes in the Si-H bond lengths. Our results correspond to Si-centered dots. However, similar changes in the CBM symmetries have been reported for dots centered on a tetrahedral interstitial site.[8]

For small and intermediate size quantum dots, we explore the influence of a departure from the geometric spherical shape on the wave-function symmetries and energy levels. We reduce the size of the dot in one direction (R_z), eliminating some atoms while keeping the size of the dot in the perpendicular plane ($R_x=R_y=$ const). For a sphere $R_z/R_x=1$. We find that the ordering of the energy levels and symmetries can change when $R_z/R_x\neq 1$. However, for sufficiently small dots, the wave functions can still be classified in terms or the representations of the T_d symmetry: for R_z/R_x as low as 0.85: because $p(\psi,\mu)$ is almost 1 or 0. For the same R_z/R_y and larger dots, this classification becomes increasingly more difficult: for $R=15$ Å and $R_z/R_x=0.85$, $p(\psi,\mu)$ values are around 0.9 and 0.1.

To check the effects of surface atomic relaxation on level-ordering, we have performed LDA calculations for the two smallest QD's reported in Table II, relaxing the atomic structure. Then we use the empirical pseudopotential method to obtain the energy levels at the LDA relaxed geometry. In the LDA calculation, we use norm-conserving pseudopotentials with a kinetic energy cutoff of 15 Ry. The initial atomic configuration is obtained from the unrelaxed bulk configuration plus a small random displacement at each atom. At the relaxed geometry we recalculated the wave functions and energies using an empirical pseudopotential approach (not LDA). We find that even in such small QD's, where surface effects are important, the effects of atomic relaxations on the electronic structure are small. The VBM t_2 symmetry of the 87-atom dot is preserved, but the symmetry of VBM of the 123-atom dot is restored from t_1 to t_2. The ordering of the conduction-band states is preserved in both cases. Though we cannot evaluate atomic relaxations for larger dots we know that such effects are going to be much smaller, because the wave functions are localized in the interior of the dot where the atomic relaxations are negligible.

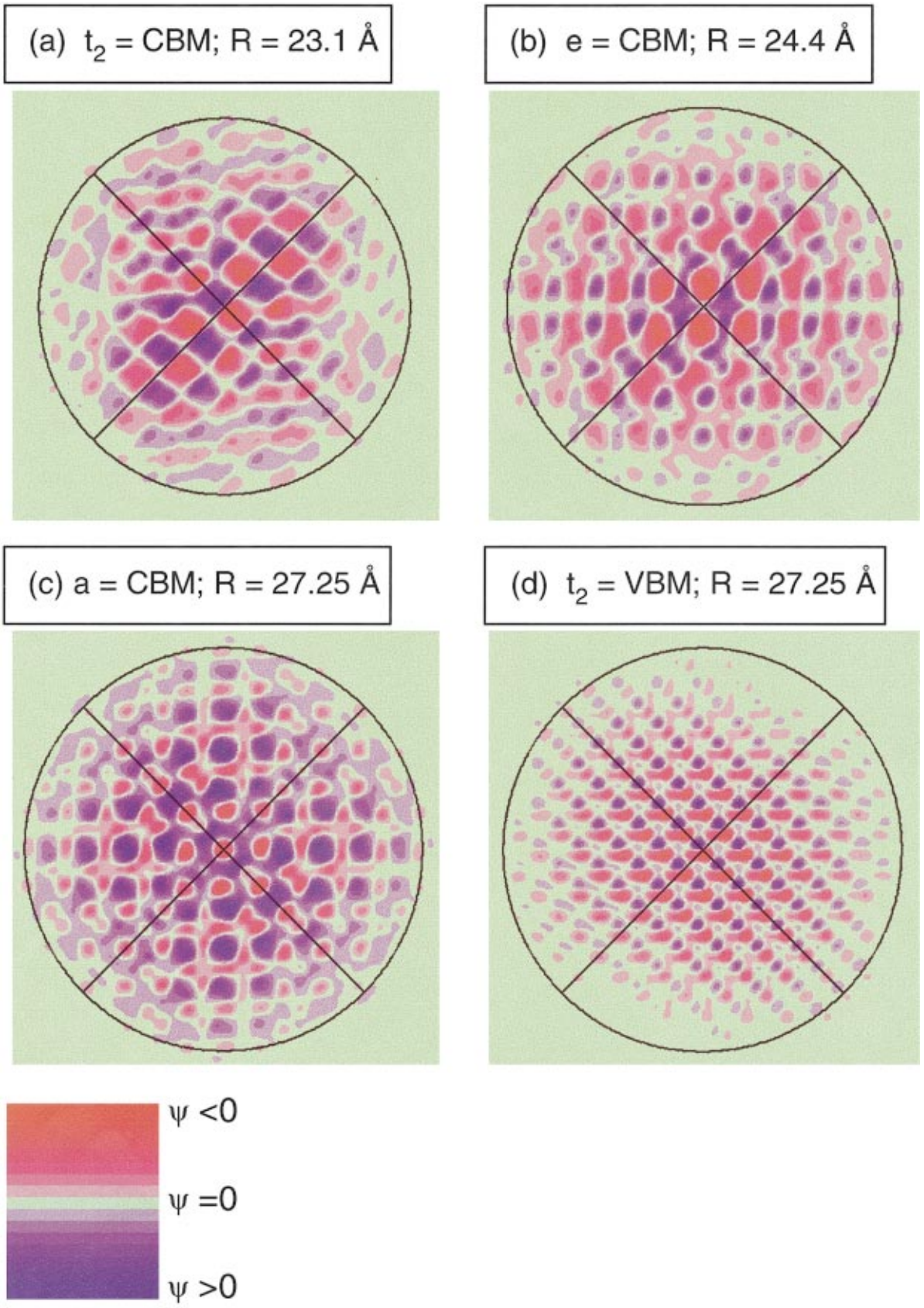

FIG. 3. (Color) Calculated wave functions, depicted along the (001) plane. Red indicates positive values, green corresponds to zero, and blue is used for negative values. The values are given in arbitrary units. The crossed solid lines correspond to the (110) and $(1\bar{1}0)$ crystallographic directions of the dot. The outer circle marks the edge of the dot.

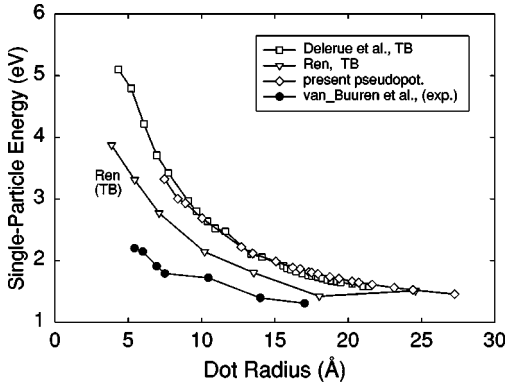

FIG. 4. Comparison between the single-particle energy gap of Si dots obtained with different theories and experiments. Squares correspond to Delerue *et al.* (Ref. 39) triangles to Ren (Ref. 7), and diamonds to the present pseudopotential calculation. Full circles correspond to the experimental data of van Buuren *et al.* (Ref. 17).

Figure 4 shows the calculated single-particle energies compared with the empirical tight-binding results of Delerue *et al.*[37] and Ren.[7] This figure shows a very good agreement with the calculation of Delerue *et al.*[37] The agreement with the calculation of Ren is not as good. The difference between the calculations of Ren and those of Delerue *et al.*[37] is that the former uses a smaller set of adjustable matrix elements in the empirical tight-binding Hamiltonian.

Also shown in Fig. 4 are the recent experimental data of van Buuren *et al.*,[17] which fall well below all calculated and measured values (see Fig. 5 below). Since the quantities measured in this experiment are very different from standard measurements,[10,11] we will review them, so as to establish if there is a relationship with calculated quantities. van Buuren *et al.*[17] measured the shift in the energy of the conduction-band minimum from the dot to the bulk, i.e.,

$$\Delta\varepsilon_{CBM}=\varepsilon_{CBM}^{dot}-\varepsilon_{CBM}^{bulk}, \tag{18}$$

and the valence-band shift

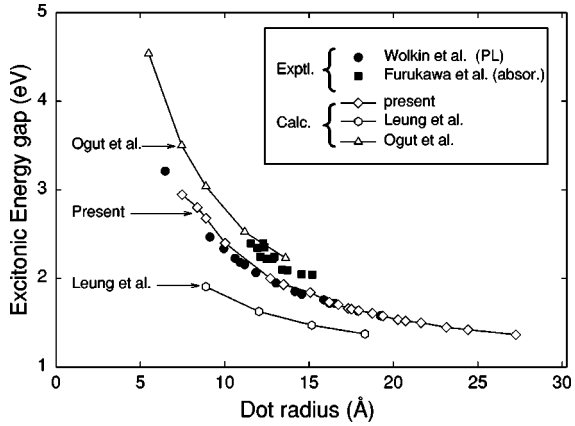

FIG. 5. Comparison between the lowest excitonic gap obtained with different theories and experiments. Full circles correspond to Wolkin *et al.* (Ref. 10), and full squares to Furukawa *et al.* (Ref. 11). Open symbols correspond to theoretical predictions: rhombus to present pseudopotential work, hexagons to Leung *et al.* (Ref. 19) tight binding and triangles to Ögüt *et al.* (Ref. 24) LDA.

$$\Delta\varepsilon_{VBM}=\varepsilon_{VBM}^{dot}-\varepsilon_{VBM}^{bulk}. \tag{19}$$

The band gap of the dot was thus

$$\varepsilon_g(dot)=\varepsilon_g(bulk)+\Delta\varepsilon_{CBM}-\Delta\varepsilon_{VBM}. \tag{20}$$

To obtain $\Delta\varepsilon_{CBM}$, van Buuren *et al.* measured the difference between $2p\rightarrow$CBM core-level absorption in the dot and in the bulk:

$$\Delta\varepsilon_{CBM}=\Delta E^{dot}(\mathrm{Si}_{2p}\rightarrow\mathrm{CBM})-\Delta E^{bulk}(\mathrm{Si}_{2p}\rightarrow\mathrm{CBM}), \tag{21}$$

whereas to obtain $\Delta\varepsilon_{VBM}$, they combined VBM photoemission with Si$2p$ photoemission, i.e.,

$$\Delta\varepsilon_{VBM}=[\Delta E^{dot}(\mathrm{VBM}\rightarrow\mathrm{vac})-\Delta E^{dot}(\mathrm{Si}_{2p}\rightarrow\mathrm{vac})]-[\Delta E^{bulk}(\mathrm{VBM}\rightarrow\mathrm{vac})-\Delta E^{dot}(\mathrm{Si}_{2p}\rightarrow\mathrm{vac})]. \tag{22}$$

In Eq. (21), $\Delta E^{dot}(\mathrm{Si}_{2p}\rightarrow\mathrm{CBM})$ is the energy difference between a dot with an electron in the CBM and a hole in its $2p$ core level and a dot in the ground state. In Eq. (22), $\Delta E^{dot}(\mathrm{VBM}\rightarrow\mathrm{vac})$ is the ionization energy of the dot VBM, and $\Delta E^{dot}(\mathrm{Si}_{2p}\rightarrow\mathrm{vac})$ is the ionization energy of the dot $2p$ core level.

It was already noted by van Buuren *et al.*[17] that the *measured* single-particle gap $\varepsilon_g(dot)$ (solid symbols in Fig. 4) obtained from Eqs. (21) and (22) are not exactly comparable to the *calculated* one-electron band gap. First, they noted that the quantity in Eq. (20) excludes the binding energy of the exciton. Second, they noted that $\Delta E^{dot}(\mathrm{Si}_{2p}\rightarrow\mathrm{CBM})$ and $\Delta E^{bulk}(\mathrm{Si}_{2p}\rightarrow\mathrm{CBM})$ correspond to energies of *core* excitons, whereas all conventional calculations of gaps in dots involve *valence* excitons. We note that because the electron wave function of a dot is localized by quantum confinement, the binding energy of a core exciton could be larger in the dot that in the bulk case. Therefore, the binding energies of the dot versus bulk core excitons will not necessarily cancel in Eq. (21), and the measured conduction band shift $\Delta\varepsilon_{CBM}$ could be underestimated relative to the single-particle result. Third, we note that in Eq. (22) the polarization energies must cancel out exactly both for a VBM hole and for a core hole in order for Eq. (22) to yield $\Delta\varepsilon_{VBM}$. Fourth, the energy level of the core electron must be assumed to be independent of the position of the Si atom (inside the dot or in the surface), and this may not be the case. In conclusion, although the experiments of van Buuren *et al.*[17] show clear evidence of quantum confinement, the physical quantities measured do not correspond to the normally calculated single-particle energies. An additional possible reason for the difference between the van Buuren *et al.*[17] measurement of the single gap and the theoretical calculations (Fig. 4) could be the fact that the dots in this experiment are touching one another and, therefore, the wave function is not confined as it is in isolated dots.[38]

B. Comparison of the calculated excitonic gaps with other theories and experiments

In Fig. 5, we compare our calculated *lowest exciton energies* with other theoretical[19,24] and experimental[10,11] studies. Our calculations correspond to the lowest excitation energy

obtained using the configuration-interaction method described in Sec. II B. The detailed structure of the exciton multiplet will be described in the next section. In Fig. 5, full symbols correspond to experimental results and open symbols correspond to theoretical predictions. We see an excellent agreement between our results and the recent photoluminescence (PL) data of Wolkin *et al.*[10] on oxygen-free samples. We also show the *absorption* data of Furukawa *et al.*,[11] used in the past to compare with theory.[24] The absorption-determined gas is much higher than the PL-determined gap for the following reason. For indirect-gap bulk semiconductors absorption does not give reliable values for the *lowest* gap (because of the small intensity); and in this case, emission is more reliable. Although the finite size of the dot breaks the translation symmetry and, in principle, the absorption is possible without the assistance of phonons, in practice the absorption coefficient is extremely small[11] at the energy threshold. Moreover, the lowest-energy exciton states can be forbidden, so absorption marks higher energy transitions, not the minimum gap. Therefore, PL (Ref. 10) is a more reliable method to locate the minimum-gap in dots made of indirect gap material (provided that nonradiative defects and surface defects are avoided.[10])

With respect to the theoretical calculations, our results also almost coincide with a empirical tight-binding calculations reported by Wolkin *et al.*[10] (which are not shown because they are on top of the experimental data). The empirical tight-binding calculations of Leung *et al.*[19] report a smaller excitonic gap, but that calculation also failed to reproduce accurately the bulk gap.[39] The LDA calculation of Ögüt *et al.*[24] agrees poorly with the experimental PL data of Wolkin *et al.*,[10] overestimating even the (already too high) absorption data of Furukawa *et al.*[11] This discrepancy results from (1) their underestimated screening function (see Fig. 2), which in turn reduces the energy of the exciton; and (2) their overestimation in the calculation of the quasi-particle energy gap,[40] which raises the energy of the exciton.

C. The excitonic multiplet spectrum

Having discussed the ''large-energy scale'' pertaining to Fig. 5, we next describe the fine structure of the excitonic spectra near the threshold. To understand the physics of exciton energies, we will calculate them in steps, introducing progressively higher order effects. (a) At zero order, the energy exciton is the difference $\varepsilon_e - \varepsilon_h$ in the single-particle energies. In this approximation one ignores all electron-hole interactions. The next step (b) is to consider a single-configuration (i.e., one diagonal block of Fig. 1) and to introduce the electron-hole direct Coulomb interaction J. This correction not only shifts the energy levels, but in indirect-gap systems, also splits the energies of the different exciton symmetries that are degenerate in the single-particle picture. Then (c) one may include the electron-hole exchange terms within a single configuration, which gives additional splittings. Finally, (d) one can add configuration interaction by solving several blocks of Eq. (11), including off diagonal terms. (e) The convergence of the exciton energies in terms of the determinantal basis set can be estimated by increasing the number of single-particle states in Eq. (11).

The symmetries of the multiplets created within each single configuration can be obtained in a straightforward manner using standard group theory. Some representative cases are given in Table I. Let us first analyze carefully some examples of the excitonic spectra of individual dots before discussing the general conclusions that apply to all the results.

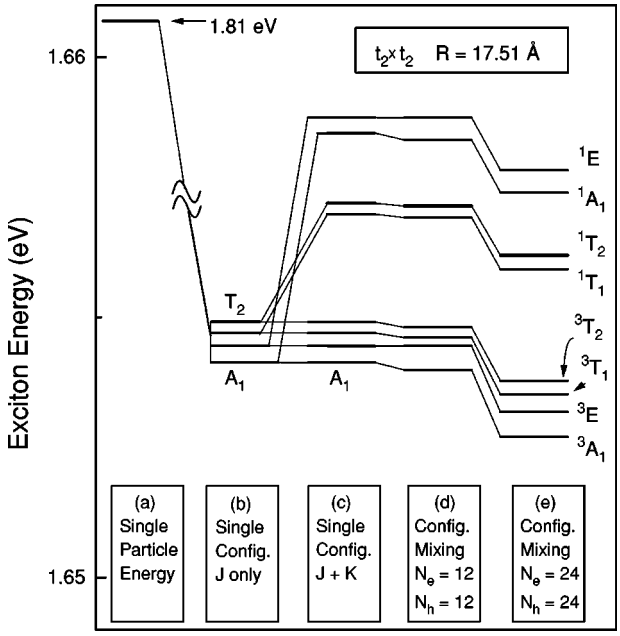

FIG. 6. Exciton energies for a dot of 1123 Si atoms $R = 17.51$ Å, calculated under different approximations [indicated in the boxed items (a)–(e)] for a $t_2 \times t_2$ configuration.

In Fig. 6, we show the energies of excitons derived from a t_2 hole and a t_2 electron state calculated at levels (a)- (e) as defined above. The results were obtained for a dot with a radius $R = 17.51$ Å. The system has 1125 Si atoms, with 436 H atoms passivating the surface dangling bonds. For clarity of display, the excitations that do not have a t_2-hole $\times t_2$-electron character are excluded from the figure. (a) At the single-particle level [Fig. 6(a)] the $t_2 \times t_2$ exciton is 36-fold degenerate. (b) The main correction to this single-particle energy is the average direct Coulomb correction $\overline{J}_{t_2 \times t_2} \sim 250$ meV [Fig. 6(b)], but this shift is not identical for every exciton in the multiplet. The Coulomb interaction splits the 36-fold degeneracy of the exciton energies into four degenerate levels denoted E, A_1, T_1, and T_2 with degeneracies 8, 4, 12, and 12, respectively. In the single configuration scheme with no exchange [Fig. 6(b)], the lowest energy exciton has A_1 symmetry and therefore is optically inactive because of the orbital selection rules even in the absence of exchange splitting. The next state E is also optically inactive. The only optically active state is the fourth one, which has T_2 symmetry. (c) The exchange contribution [Fig. 6(c)] splits the energy of each exciton level in singlet and triplet states, with latter optically inactive. However, the energy shift between singlet and triplet excitons depends on the orbital symmetry: it is much larger for A_1 and E excitons than for T_1 and T_2. As a consequence, the lowest energy singlet exciton has T_1 symmetry and is optically inactive, whereas the next singlet exciton is T_2 and is active. (d) Correlation effects are taken into account in Figs. 6(d) and 6(e). In this dot, multiple configuration interactions *do not* alter

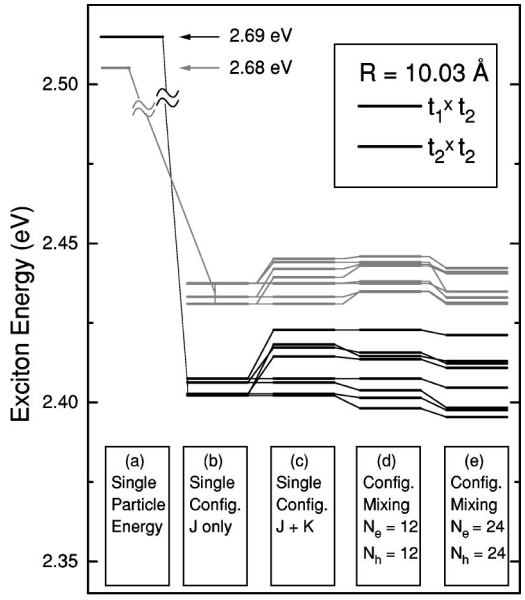

FIG. 7. Exciton energies of a dot of 211 Si atoms $R = 10.03$ Å, calculated under different approximations indicated in the boxed items (a)–(e). Note the crossing between the $t_2 \times t_2$ and the $t_1 \times t_2$-related excitations resulting from the direct Coulomb corrections.

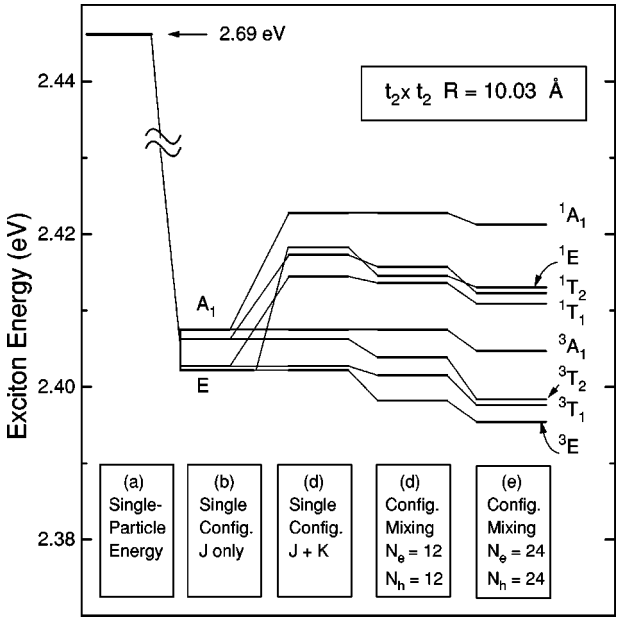

FIG. 8. The $t_2 \times t_2$ exciton manifold of Fig. 7 given on a larger scale.

the ordering of the energy levels and they introduce energy correction on the order of 1 meV only.

Because the lowest energy exciton has A_1 symmetry, the exciton is dark, which results from both the exchange interaction and the direct Coulomb contribution of the Coulomb interaction. Therefore, an exciton in the ground state has to flip the spin and also has to change the orbital symmetry in order to recombine in a dipolar transition. That means that the exciton transition is forbidden both by spin and orbital symmetry. However, spin-orbit coupling, which is not included in the present calculation, can partially mix singlet and triplet states.

Another example of dark exciton is shown in Figs. 7 and 8 for a much smaller dot. The QD has 211 Si atoms with additional 140 H atoms on its surface. The effective radius of the Si dot is $R = 10.03$ Å. The symmetry of the VBM for this dot is t_1, whereas the CBM is t_2 (see Table II). In the absence of e-h interaction [Fig. 7(a)], this $t_1 \times t_2$ exciton is 36-fold degenerate. Surprisingly, we find that the lowest energy exciton does not belong to a $t_1 \times t_2$ multiplet. The reason is that the hole state next to the VBM state has t_2 symmetry and is only 10 meV below the $t_1 -$VBM. The difference between $\overline{J}_{t_2 \times t_2}$ and $\overline{J}_{t_1 \times t_2}$ is large enough to displace the exciton energy of the $t_2 \times t_2$ multiplet below the $t_1 \times t_2$ [Fig. 7(b)]. Thus, the low-energy excitonic multiplets are derived from t_2 holes even though the t_1 holes are higher in energy. Figure 8 shows the exciton obtained from the $t_2 \times t_2$ multiplet on an enlarged scale. In this dot, the direct Coulomb interaction is able to lower the energy of a dark exciton E below the optically active T_2 exciton [Fig. 8(b)]. But, as in the example of Fig. 6, the exchange splitting [Fig. 8(c)] is smaller for the T singlets than for A_1 and E singlets. For this reason the symmetry of the lowest energy singlet [Fig. 8(c)] is T_1 whereas the next singlet state is T_2. In contrast with the previous example, in this case configuration-mixings are important [Figs. 8(d) and 8(e)], and energy corrections are much larger. As a consequence, they can interchange the ordering of the exciton symmetries. This is due not only to the proximity of the $t_1 \times t_2$ and $t_2 \times t_2$ configurations, but also, to the relative growth of the values of the of diagonal matrix elements in Eq. (11) (see below).

Figures 6, 7, and 8 clearly show that the excitonic transitions are degenerate at the single-particle level. Therefore, errors in the single-particle energies do not play a significant role in the values of the splittings in a multiplet. However, they can rigidly shift the full multiplet. We have found that (1) when the CBM has t_2 symmetry, the direct Coulomb interaction gives rise to a dark exciton. However, (2) when the symmetry of the CBM is ''e,'' the lower energy exciton is in general T_2, which is bright. Finally, (3) when the CBM symmetry is a_1 the exciton always has T_2 symmetry. Changes in the screening function (as large as those occurring when the size of the dot changes form 8 to 27 Å) do not alter the main conclusion of this work: the excitonic transition is symmetry forbidden when the symmetry of the CBM is t_2 and allowed when it is not.

Unfortunately, the present experimental resolution and size distribution of real samples does not allow us to resolve splittings as small as the ones introduced by the Coulomb interaction by direct PL experiments. Future single-dot experiments are necessary to examine our predictions of Figs. 6 and 8.

D. Bright-dark exciton splitting as a function of the exciton energy

We next compare the calculated and measured splitting between the dark and bright excitons. There are two types of experiments in this regard: ''optical''[41] and ''thermal.''[41–43] In the *optical* experiment, one absorbs light into the optically

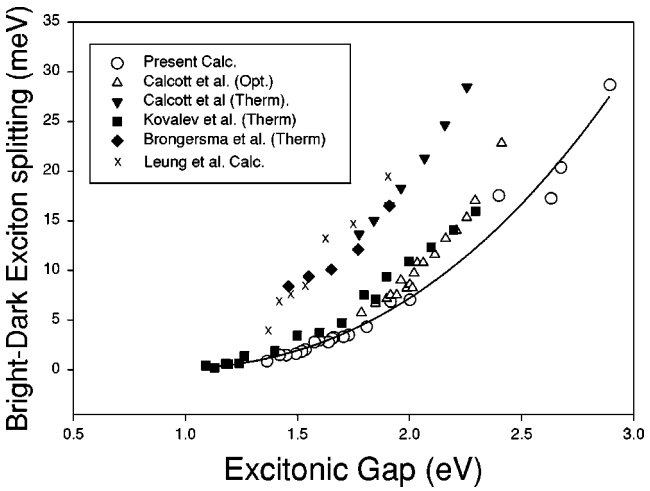

FIG. 9. Energy-splitting between the lowest-energy bright exciton and the lowest-energy dark exciton as a function of the dark-exciton energy. Circles correspond to the present calculations and crosses to the results of Leung *et al.* (Ref. 19); the solid continuous line is a guide to the eye. Open and closed triangles correspond, respectively, to the optical onset measurements and thermal PL decay measurements of Calcott *et al.* (Ref. 41); squares correspond to the thermal PL decay measurements of Kovalev *et al.* (Ref. 42); diamonds correspond to the thermal PL decay measurements of Borngersma *et al.* (Ref. 43).

allowed state (i.e., ${}^1T_2$), and emits from the lowest-energy triplet (e.g., ${}^3A_1$ in Fig. 6) or from a thermal average over the lowest-energy triplets. The absorption versus emission Stokes shift then corresponds to the sum $\delta_{opt}=\Delta+\Delta_{\rm FC}$ of two effects: the bright-dark (''singlet-triplet'') splitting Δ and the Franck-Condon shift $\Delta_{\rm FC}$ due to the possibility that the atomic geometry in the excited state differs from that in the ground state. Note that in Si QD's, Δ does not necessarily correspond to an ''exchange splitting'' because the *orbital* symmetry of the bright and dark states might be different. Consequently, Δ contains also electron-hole Coulomb terms.

In a *thermal* experiment[41–43] the radiative decay rate of singlet to ground state and triplet to ground state is measured as a function of the temperature T. When k_BT is much smaller than δ_{th}, only the lower-energy forbidden triplet states are populated and the radiative decay is small. On the other hand, when k_BT is of the order of δ_{th} or larger, the occupation of the allowed ${}^1T_2$ states increases. As a result of the larger occupation of the optically allowed states, the radiative decay rate increases. The experimental works[41–43] fit the radiative decay rate to a two-level (singlet-triplet) model in which δ_{th} is an adjustable parameter. Since the atomic geometry is expected to be very similar in the excited singlet and the excited triplet there is no Franck-Condon contribution to the thermally measured Shift δ_{th}.

The values obtained for δ_{opt} and δ_{th} in the thermal and optical experiments[41–43] are summarized in Fig. 9 along with the tight-binding calculations of Leung *et al.*,[19] and the present pseudopotential results, as a function of the exciton energy.

We see in Fig. 9 that (1) the optical shift δ_{opt} of Calcott *et al.*[41] and the thermal data of Kovalev *et al.*[42] agree very well with each other, but differ from the thermal results δ_{th} of both Calcott *et al.*[41] and Brongersma *et al.*[43] It has been argued by Calcott *et al.*[41] that shape distributions might justify the difference between their optical and thermal experiments. However, our calculated exchange energies and single-particle energies show that they are dependent on the volume of the dots rather than their shape. Because, the exchange energy and the single-particle energy are the main contributors to the dark-bright splittings and excitonic gaps, respectively, we think that small shape fluctuations cannot account for the difference between optical and thermal experiments[41] or between different thermal experiments.[41–43]

(2) The qualitative agreement between different theories and experiments is good. Our calculations are in excellent quantitative agreement with the optical δ_{opt} onset measurements of Calcott *et al.*,[41] and the variable-temperature measurements of Kovalev *et al.*[42] The thermal data of Calcott *et al.*[41] and Brongersma *et al.*[43] are both a factor of 1.8 higher than our calculations. The theoretical calculations of Leung *et al.*[19] are only slightly above the thermal data of Calcott *et al.*[41] and Brongersma *et al.*[43] The results of Martin *et al.*[44] (not shown) only fit the experimental data when an artificially low-dielectric constant is used.

(3) The fact that the calculated bright-dark splitting agrees with the optical shift $\delta_{opt}=\Delta+\Delta_{\rm FC}$ between absorption and emission does not leave much room for a Franck-Condon shift $\Delta_{\rm FC}$. Indeed, the total measured shift $\Delta+\Delta_{\rm FC}\lesssim 10$ meV is much smaller than Franck-Condon shift in large molecules ($\Delta_{\rm FC}\gtrsim 100$ meV). Another puzzle is the fact that the measured thermal shift $\delta_{th}\approx\Delta$ is *larger* that the measured optical shift $\delta_{opt}=\Delta+\Delta_{\rm FC}$.

(4) Figure 9 plots the dark-bright energy splittings $\Delta(R)$ versus the excitonic gap energy $\varepsilon_g^{opt}(R)$. Although the $\Delta(R)$ vs $\varepsilon_g^{opt}(R)$ plot of Leung *et al.* lies well above ours, their $\Delta(R)$ values for a given dot radius R agree with our values. In fact, the $\Delta(R)$ vs $\varepsilon_g^{opt}(R)$ plot of Leung *et al.*[19] is shifted to smaller ε_g^{opt} values with respect to our values. This is because their absolute excitonic energies are lower than ours (see Fig. 5), which can be traced to the fact that their single-particle levels are much lower too. Indeed, it has been noted recently[39] that the tight-binding Hamiltonian used by Leung *et al.*[19] might give single-particle band gaps that are too low. We estimate that Leung *et al.*[19] results would be almost identical to our results in Fig. 9 if their single-particle gaps were similar to those reported by Delerue *et al.*[37]

Another question is if the electron-phonon interactions can mix exciton levels. If the excited state distortions are small, one could treat both the electronic and the phonon Hamiltonian in the same quantum mechanical approach. Because all lattice distortions that are symmetry equivalent (e.g., x, y, z) cost the same energy, the effective electron-hole phonon coupling Hamiltonian due to lattice distortions must have the symmetry of the dot. Therefore, this effective Hamiltonian will not mix different representations of the exciton wave function (e.g., T_1 with T_2), although it could contribute to the Coulomb splittings (e.g., energy splitting between T_1 and T_2). On the other hand, if excited state distortions are large (i.e., if the frequency square of one or more phonons becomes negative in the excited state geometry[45,46]) the symmetry of the electronic Hamiltonian could be broken after atomic relaxation and thus exciton lev-

els of different symmetry could be mixed. A comparison between optical experiments and our theoretical results seems to show that the Franck-Condon shifts are small. Accordingly, we suspect that additional splittings or mixings due to lattice distortion should be small compared to the Coulomb or exchange splittings.

IV. SIZE DEPENDENCE OF THE SINGLE-PARTICLE AND INTERACTION ENERGIES

It is important to compare the size scaling of the single-particle gap $\varepsilon_g \sim R^{-n}$ with the size scaling of the electron-hole Coulomb interaction $J \sim R^{-m} R$. If ε_g grows faster than J as $R \to 0$, then Coulomb effects become negligible as compare with single-particle energies at small sizes. On the other hand, if J grows faster than ε_g for $R \to 0$, the importance of correlation effects increases.

A. Size scaling of the single-particle energies

The single-particle energy gap is usually fit with a function of the form

$$\varepsilon_g = \varepsilon_g^{bulk} + \beta / R^{\gamma}, \tag{23}$$

where $\varepsilon_g^{bulk} = 1.17$ is the single-particle gap in bulk silicon. Using Eq. (23) and all values of Table II, our fitted value for γ is 1.42. (If we restrict the data to the dots studied by Wang and Zunger[22] $R \leqslant 18.75$ Å we get $\gamma = 1.37$, the same as they do.) For large dots, when the EMA is valid, it is expected that $\gamma(R \to \infty) = 2$. Therefore, a more general fitting function that allows γ to be a function of the dot size R is required:

$$\varepsilon_g = \varepsilon_g^{bulk} + \beta / R^{\gamma(1+\delta R)}, \tag{24}$$

where δ is a small additional fitting parameter that allows the exponent to change as a function of R. A fit by Eq. (24) shows that the quantity $\gamma(1+\delta R)$ is 1.13, 1.20, and 1.27 for $R = 7$, 17, and 27 Å, respectively. This means that the ''exponent'' of R is a strong function of the size R itself. Accordingly, disagreements between different theories can be partially understood by the different size of the dots studied. Our exponents are larger than the value obtained by Delley *et al.*[8] ($\gamma = 1$) using LDA, but are similar to the value $\gamma = 1.39$ obtained by Proot *et al.*[20] and $\gamma = 1.37$ by Wang *et al.*[22] The average size scaling of the CBM energy is $R^{-1.4}$ and for the VBM energy it is $R^{-1.0}$. Thus, the low exponent of the single-particle gap is mainly a consequence of the smoother dependence of the VBM on size.

B. Symmetrization of the Coulomb and exchange integrals

It is advantageous to combine certain exchange and direct Coulomb integrals for the purpose of analyzing their size scaling (but not for calculation). For degenerate states, the solution of Eq. (1) gives a set of wave functions. Any linear combination of these wave functions is also a possible solution of the single-particle Eq. (1). The numerical method used to diagonalize H can select any set of orthogonal linear combinations of the degenerate wave functions as a solution. Because the values of a particular matrix element $J_{he,h'e'}$ or $K_{he,h'e'}$ depend on the (arbitrary) linear combination of the degenerate conduction and valence band levels, they are not suitable for analyzing the dependence of J and K as a function of the dot size. To do this, we first diagonalize the matrixes $J_{he,h'e'}$ or $K_{he,h'e'}$ in the subspace of a given single configuration, obtaining the eigenvalues $j_{he}(C)$ and $k_{he}(C)$, respectively

$$Q J_C Q^{-1} = j_{he}(C)\, \delta_{h,h'} \delta_{e,e'}, \tag{25}$$

and

$$T K_C T^{-1} = k_{he}(C)\, \delta_{h,h'} \delta_{e,e'}; \tag{26}$$

where C represents electron-hole pairs of the form $h \times e$ [a shaded block (Fig. 1)], J_C and K_C are single-configuration submatrixes of the full matrixes $J_{he,h'e'}$ or $K_{he,h'e'}$, and Q and T are unitary transformation matrices. We take the average value of the direct Coulomb and exchange interactions $\overline{J_C}$ and $\overline{K_C}$ as a measure of the strength Coulomb interaction in a given configuration:

$$\overline{J_C} = \frac{1}{N_c} \sum_{he} j_{he}(C), \tag{27}$$

$$\overline{K_C} = \frac{1}{N_s} \sum_{s} k_{he}(C). \tag{28}$$

In Eq. (28), the average is taken on the N_s singlet states that have $k_{he}(C)$ eigenvalues different from zero (singlet states). The splitting in energy of the eigenvalues $j_{he}(C)$ and $k_{he}(C)$ is a consequence of the exciton-exciton couplings within each configuration C. Accordingly, they are a good measure of the exciton-exciton interaction within a configuration. We then define

$$\Delta \overline{J_C} = \frac{1}{N_c} \sum_{he} |j_{he}(C) - \overline{J_C}| \tag{29}$$

$$\Delta \overline{K_C} = \frac{1}{N_s} \sum_{s} |k_{he}(C) - \overline{K_C}|. \tag{30}$$

Equations (27) and (28) are functions of the traces of the matrices while Eqs. (29) and (30) are only dependent on the basis where $J(C)$ or $K(C)$ are diagonal within each configuration. Therefore, they are independent of the particular choice of the degenerate single-particle states. The symmetry of the band-edges extrema depends on the dot size. For that reason, we did not limit our study to the evolution of the band-edge transitions; we also followed each configuration and characterized their direct Coulomb and exchange dependence independently as a function of the dot radius.

C. Comparison between scaling behaviors

In order to study the relative importance of the direct Coulomb and exchange interaction as a function of the dot radius, we evaluated Eqs. (27), (28), (29), and (30) for all the dots in Table II. Using a least-squares procedure, we fit Eq. (27) with a function of the form:[47]

$$\overline{J_C}(R) = \alpha + \beta / R^{\gamma}, \tag{31}$$

and Eq. (28) with a function of the form

TABLE III. Size scaling of the direct Coulomb and exchange contribution ($R^{-\gamma}$) as defined in Eqs. (31) and (32). Cases a–f refers to Table I.

Case	γ in $\bar{J}_C$	γ in $\Delta\bar{J}_C$	γ in $\bar{K}_C$	γ in $\Delta\bar{K}_C$
a	1.49	1.94	2.71	2.53
b	1.46		2.72	
c	1.49	1.93	2.67	2.48
d	1.36	2.57	2.71	2.31
e	1.28		2.31	
f	1.29	3.0	2.50	2.17

$$\Delta\bar{J}_C(R) = \beta/R^{\gamma}. \tag{32}$$

The form of Eq. (32) is also used to obtain the fits $\bar{K}_C(R)$, and $\Delta\bar{K}_C(R)$ of Eqs. (29) and (30). Table III gives the values of the exponent γ obtained from the fittings.

The first observation is that the exponent obtained for the size scaling of the direct-screened Coulomb energy $J_C \sim R^{-1.49}$ is larger than the one obtained in simplified models that use a size-independent screening constant and the EMA: $J \sim R^{-1}$. Note from Eq. (9) that the scaling of J depends on the wave function structure and on the scaling of $\bar{\epsilon}(r,R)$. In our calculation, the wave function is not constrained to be zero at the surface of the dot, which is the usual boundary condition for the envelope wave function in free-standing QD's. This leads to a *reduced*[48] electron-hole binding energy, so the unscreened Coulomb energy scales as $J(unscreened) \sim R^{-0.82}$. On the other hand, our $\bar{\epsilon}(r,R)$ depends on the dot size being smaller than the $R \to \infty$ bulk value [see Eq. (16) and Fig. 2]. This effect *increases* the electron-hole binding energy. The combination of both effects produces the final result as $J(screened) \sim R^{-1.49}$.

Because $\varepsilon_g \sim R^{-1.2}$, the relative importance of the Coulomb interaction compared to the single-particle gap is larger for the smaller dots than for the larger ones. This directly contradicts the assumption of simplified models[32,26] about the relative importance of single-particle energies and Coulomb energies in small dots.

The consequences of these scaling behaviors are evident from a comparison among Figs. 6, 7, and 8. The average direct Coulomb correction in Fig. 7(b) is large enough to change the order of the excitonic transitions from the calculated single-particle energies in Fig. 7(a). In addition, Fig. 8 shows that configuration interactions are large enough to disturb the order of the exciton energies [see Figs. 8(c), 8(d), and 8(e)]. This is a consequence of the larger influence of electron-hole correlations [included in Figs. 8(d) and 8(e)] in very small dots. On the other hand, when the size of the dot becomes comparable with the bulk Bohr radius, correlation effects become crucial, because the exciton becomes localized by the Coulomb interaction itself and not by quantum confinement.

The second observation from Table III is that, in every case, the exchange integrals decay much faster than the direct Coulomb integrals. Then, for small systems, the singlet-triplet splitting is much larger than the direct Coulomb splittings. However, for large enough dots, the splittings introduced by the direct Coulomb interaction itself become of the same order of magnitude as singlet-triplet splittings. The fact that $\gamma \approx 3$ for $\bar{K}_C(R)$ means that, for indirect gap material, the exchange integrals are given basically by the short-range contribution.[1]

Finally, we note that in Table III the electron-hole excitations can be classified in two groups in which the direct Coulomb interaction has distinct scaling properties. Group I has t_2 hole wave functions, whereas group II has t_1 holes. $\bar{J}_C$ has stronger dependence on the dot radius for group I excitons than for group II (see Table III). The difference in $\bar{J}_C(R)$ between I and II groups tends to zero for large enough QD's. Thus, for small dots, $\bar{J}_C$ is much larger for group-I transitions than for group II. For that reason, the direct Coulomb term in Fig. 7(b) is large enough to compensate the energy crossing between the t_1 and t_2 solutions in the valence band. As a result, the lower-energy exciton has group-I character for all but one of the dots listed in Table II. The only exception is the third dot in Table II. In this case. excitations belonging to group I and II are superimposed. Therefore, the interexciton coupling due the direct Coulomb and exchange interactions becomes more important, and the lower exciton has only an impure group-II character. Nevertheless, in this small size regime the VBM symmetry becomes uncertain because relaxation effects tend to restore the t_2 symmetry of the VBM.

The Coulomb integrals in group I have similar dependence on R (see Table III). This result is expected, because the lowest electron states are the a_1, e, and t_2 states formed from the six degenerate minima of the bulk-conduction band structure.[7] Consequently, the Bloch parts of the wave functions are similar and give similar matrix elements. As a consequence, the symmetries of the lower-energy exciton multiplet are fixed by the symmetry of the CBM, even though the single-particle energy splittings in the conduction band are much smaller than the average direct Coulomb energy.

D. The origin of nonclassical size-scaling

The classical size scaling of

$$\varepsilon_g \propto R^{-2} \tag{33}$$

assumes (a) single-band theory, (b) parabolic bands, and (c) infinite barriers. Recently Ferreyra and Proetto[49] have demonstrated that exponents smaller than the classic values of Eq. (33) can be obtained in a single-band theory with parabolic bands, provided that one replaces the infinite potential barrier by some finite potential barrier. This result does not clarify the relative physical origins (a)–(c) of the nonclassic exponents. Our present EPM calculations includes all three contributions (a)–(c) to the value of the exponents. The fact that not only finite barriers, but also nonparabolicity contribute to the value of the exponent can be gleamed from the following: In the ''truncated crystal'' (TC) calculation,[50] one replaces the parabolic band approximation by the actual nonparabolic bands of the host material, while retaining the single-band description. It was found[50] that the exponent $\varepsilon_g \propto R^{-n}$ is already much smaller than the classic value of $n = 2$ even though both the single-band approximation and the

infinite potential barrier approximation were used. Thus, nonparabolicity of the bulk band reduces n.

V. CONCLUSIONS

We have found that Coulomb interactions are very important in determining the symmetry of excitons in quantum dots made of a bulk indirect-gap material. In particular, (1) direct Coulomb interactions are able to split the energies of excitons that have degenerate single-particle energies. (2) When the symmetry of the CBM is t_2, the direct Coulomb interaction lowers the energy of a dark exciton below the optically active ones. (3) Exchange corrections raise the energy of singlet states; because exchange splittings are different for each exciton symmetry, the ordering of symmetries is altered by the exchange interaction. In general, the exchange splitting is smaller for T singlets than for E or A_1, which lowers their energies below the other singlets. But, the T_2 singlet remains at higher energy than the T_1. (4) When the symmetry of the CBM is not t_2, the lower energy excitons have T_2 symmetry. Thus, when the CBM symmetry is not t_2, the lowest exciton is spin-forbidden only. (5) The hole wave function of the lowest-energy exciton belongs to the t_2 symmetry even in some cases in which the symmetry of the VBM is t_1. This is due to the fact that, for small dots, the electron-hole direct Coulomb attraction is significantly larger when the hole is t_2 than when it is t_1. (6) We find that our dark-bright excitonic splitting agrees very well with the experimental optical data of Calcott *et al.*[41] and thermal data Kovalev *et al.*[42] The agreement is not as good with the thermal data of Calcott *et al.*[41] and Brongersma *et al.*[43] Finally, (7) in contradiction with simple textbook arguments, we have found that the relevance of the Coulomb direct interaction, exchange interaction, and correlation effects increase as compared to the single-particle energy splittings for smaller dots. This effect is a consequence of a realistic description of the dot potential and the interparticle screening.

ACKNOWLEDGMENTS

The authors would like to thank Lin-Wang Wang for supplying some of the programs used in this work and for stimulating discussions. The authors also would like to thank D. Kovalev and M. Brongersma for supplying their bright-dark exciton shifts (Fig. 9) prior to publication. This work was supported by OER-BES-DMS under Contract No. DE-AC36-98-GO10337.

[1] A. Franceschetti, L. W. Wang, H. Fu, and A. Zunger, Phys. Rev. B **58**, R13 367 (1998).
[2] Al. L. Efros, M. Rosen, M. Kuno, M. Nirmal, D. J. Norris, and M. Bawendi, Phys. Rev. B **54**, 4843 (1996).
[3] H. Fu and A. Zunger, Phys. Rev. B **57**, R15 064 (1998).
[4] U. Banin, C. J. Lee, A. A. Guzelian, A. V. Kadavanich, A. P. Alivisatos, W. Jaskolski, G. W. Bryant, Al. L. Efros, and M. Rosen, J. Chem. Phys. **109**, 2306 (1998).
[5] M. Chamarro, M. Dib, V. Voliotis, A. Filoramo, P. Roussignol, T. Gacoin, J. P. Boilot, C. Delerue, G. Allan, and M. Lannoo, Phys. Rev. B **57**, 3729 (1998).
[6] A. Franceschetti and A. Zunger, Appl. Phys. Lett. **68**, 3455 (1996).
[7] S. Y. Ren, Phys. Rev. B **55**, 4665 (1997).
[8] B. Delley and E. F. Steigmeier, Phys. Rev. B **47**, 1397 (1993).
[9] S. Y. Ren, Solid State Commun. **102**, 479 (1997).
[10] M. V. Wolkin, J. Jorne, P. M. Fauchet, G. Allan, and C. Delerue, Phys. Rev. Lett. **82**, 197 (1999).
[11] S. Furukawa and T. Miyasato, Phys. Rev. B **38**, 5726 (1988).
[12] L. Zhang, J. L. Coffer, and T. W. Zerda, J. Sol-Gel Sci. Technol. **11**, 267 (1998).
[13] D. Kovalev, H. Heckler, M. Ben-Chorin, G. Polisski, M. Schwartzkopff, and F. Koch, Phys. Rev. Lett. **81**, 2803 (1998).
[14] B. H. Choi, S. W. Hwang, I. G. Kim, H. C. Shin, Yong Kim, and E. K. Kim, Appl. Phys. Lett. **73**, 3129 (1998).
[15] H. Kohno and S. Takeda, Appl. Phys. Lett. **73**, 3144 (1998).
[16] J. P. Wilcoxon, G. A. Samaram, and P. N. Provencio, Phys. Rev. B **60**, 2704 (1999).
[17] T. van Buuren, L. N. Dinh, L. L. Chase, W. J. Siekhaus, and L. J. Terminello, Phys. Rev. Lett. **80**, 3803 (1998).
[18] N. A. Hill and K. B. Whaley, Phys. Rev. Lett. **75**, 1130 (1995).
[19] K. Leung and K. B. Whaley, Phys. Rev. B **56**, 7455 (1997).
[20] J. P. Proot, C. Delerue, and G. Allan, Appl. Phys. Lett. **61**, 1948 (1992).
[21] M. V. Rama Krishna and R. A. Friesner, Phys. Rev. Lett. **67**, 629 (1991).
[22] L. W. Wang and A. Zunger, in *Semiconductor Nanostructures*, edited by P. V. Kamat and D. Meisel (Elsevier Science B.V., New York, 1996), Vol. 103.
[23] L. W. Wang and A. Zunger, Phys. Rev. Lett. **73**, 1039 (1994).
[24] S. Ögüt, J. Chelikowsky, and S. Louie, Phys. Rev. Lett. **79**, 1770 (1997).
[25] M. Lannoo, C. Delerue, and G. Allan, Phys. Rev. Lett. **74**, 3415 (1995).
[26] T. Takagahara and K. Takeda, Phys. Rev. B **53**, R4205 (1996).
[27] S. B. Zhang, C. Y. Yeh, and A. Zunger, Phys. Rev. B **48**, 11 204 (1993).
[28] M. Hamermesh, *Group Theory and Its Applications to Physical Problems* (Dover, New York, 1989).
[29] A. Franceschetti, H. Fu, L. W. Wang, and A. Zunger, Phys. Rev. B **60**, 1819 (1999).
[30] C. Kittel, *Quantum Theory of Solids* (John Wiley & Sons, New York, 1963), p. 101.
[31] R. Resta, Phys. Rev. B **16**, 2717 (1977).
[32] L. E. Brus, J. Chem. Phys. **79**, 5566 (1983); *ibid.* **80**, 4403 (1984); G. Allan, C. Delerue, M. Lannoo, and E. Martin, Phys. Rev. B **52**, 11 982 (1995).
[33] P. Bolcatto and C. R. Proetto, Phys. Rev. B **59**, 12 487 (1999).
[34] L. J. Sham and T. M. Rice, Phys. Rev. **144**, 708 (1966).
[35] V. A. Kiselev and A. G. Zhilich, Fiz. Tverd. Tela (Leningrad) **14**, 1438 (1972) [Sov. Phys. Solid State **14**, 1233 (1972)]; **15**, 1351 (1972) [**15**, 2024 (1973)].
[36] In Resta's paper, the screening function for semiconductors is obtained by requiring it to be a constant value for large r. This condition is satisfied for r larger than the screening radius ρ_∞. Accordingly, the approach followed by Resta (Ref. 31) is applicable for a dot much larger than ρ_∞. However, this might not be

good to describe the surface region (i.e., when the distance from one particle to the surface of the dot is on the order of ρ_∞). Nevertheless, the wave functions are strongly localized in the interior of the dots and, therefore, any correction introduced at the surface must be small.

[37] C. Delerue, M. Lannoo, and G. Allan, J. Lumin. **57**, 249 (1993).

[38] T. van Buuren (private communication).

[39] C. Delerue, M. Lannoo, and G. Allan, Phys. Rev. Lett. **76**, 3038 (1996).

[40] A. Franceschetti, L.-W. Wang, and A. Zunger, Phys. Rev. Lett. **83**, 1269 (1999).

[41] P. D. Calcott, K. J. Nash, L. T. Canham, M. J. Kane, and D. Brumhead, J. Phys.: Condens. Matter **5**, L91 (1993).

[42] D. I. Kovalev, H. Heckler, G. Polisski, and F. Koch, Phys. Status Solidi B **215**, 871 (1999).

[43] M. L. Brongersma, P. G. Kik, A. Polman, K. S. Min, and H. A. Atwater, Appl. Phys. Lett. **76**, 351 (2000).

[44] E. Martin, C. Delerue, G. Allan, and M. Lannoo, Phys. Rev. B **50**, 18 258 (1994).

[45] R. J. Baierle, M. J. Caldas, E. Molinari, and S. Ossicini, Solid State Commun. **102**, 545 (1997).

[46] G. Allan, C. Delerrue, and M. Lannoo, Phys. Rev. Lett. **76**, 2961 (1996).

[47] The coefficient α is left free in Eq. (31) to allow γ to give the average exponent of the size scaling within the radii studied only.

[48] A. Franceschetti and A. Zunger, Phys. Rev. Lett. **78**, 915 (1997).

[49] J. M. Ferreyra and C. Proetto, Phys. Rev. B **60**, 10 672 (1999).

[50] A. Franceschetti and A. Zunger, J. Chem. Phys. **104**, 5572 (1996).